Discovery of compounds that inhibit SARS-CoV-2 Mac1-ADP-ribose binding by high-throughput screening

Anu Roy[a,*], Yousef M. Alhammad[b,*], Peter McDonald[a], David K. Johnson[c], Junlin Zhuo[d], Sarah Wazir[e], Dana Ferraris[f], Lari Lehtiö[e], Anthony K.L. Leung[d], Anthony R. Fehr[b,#]

*These authors contributed equally to this work

[a]Infectious Disease Assay Development Laboratory/HTS, University of Kansas, Lawrence, Kansas 66047, USA
[b]Department of Molecular Biosciences, University of Kansas, Lawrence, Kansas 66045, USA
[c]Molecular Graphics and Modeling Laboratory and the Computational Chemical Biology Core, University of Kansas, Lawrence, Kansas 66047, USA
[d]Department of Biochemistry and Molecular Biology, Bloomberg School of Public Health, Johns Hopkins University, Baltimore, Maryland 21205, USA
[e]Faculty of Biochemistry and Molecular Medicine & Biocenter Oulu, University of Oulu, Oulu, Finland
[f]McDaniel College Department of Chemistry, 2 College Hill, Westminster, MD [a]McDaniel College, Westminister, MD 21157

[#]Correspondence: arfehr@ku.edu; Tel.: +1- (785) 864-6626 (K.S.)

Running title: Discovery of SARS-CoV-2 Mac1 Inhibitors

Keywords: Coronavirus, SARS-CoV-2, macrodomain, ADP-ribose, ADP-ribosylation, high-throughput screening

26 **ABSTRACT**

27   The emergence of several zoonotic viruses in the last twenty years, especially the

28 pandemic outbreak of SARS-CoV-2, has exposed a dearth of antiviral drug therapies for viruses

29 with pandemic potential. Developing a diverse drug portfolio will be critical for our ability to

30 rapidly respond to novel coronaviruses (CoVs) and other viruses with pandemic potential. Here

31 we focus on the SARS-CoV-2 conserved macrodomain (Mac1), a small domain of non-structural

32 protein 3 (nsp3). Mac1 is an ADP-ribosylhydrolase that cleaves mono-ADP-ribose (MAR) from

33 target proteins, protects the virus from the anti-viral effects of host ADP-ribosyltransferases, and

34 is critical for the replication and pathogenesis of CoVs. In this study, a luminescent-based high-

35 throughput assay was used to screen ~38,000 small molecules for those that could inhibit Mac1-

36 ADP-ribose binding. We identified 5 compounds amongst 3 chemotypes that inhibit SARS-CoV-

37 2 Mac1-ADP-ribose binding in multiple assays with IC_{50} values less than $100\mu M$, inhibit ADP-

38 ribosylhydrolase activity, and have evidence of direct Mac1 binding. These chemotypes are

39 strong candidates for further derivatization into highly effective Mac1 inhibitors.

INTRODUCTION

COVID-19, caused by severe acute respiratory syndrome coronavirus 2 (SARS-CoV-2), is one of the most disruptive and deadly pandemics in modern times, with greater than 385 million cases and having led to greater than 5.7 million deaths worldwide. SARS-CoV-2 is the third CoV to emerge into the human population in the last 3 decades, following outbreaks of SARS-CoV in 2002-2003 and Middle East respiratory syndrome MERS-CoV in 2012. These outbreaks highlight the potential for CoVs to cross-species barriers and cause severe disease in a new host. There is a tremendous need to develop broad-spectrum antiviral therapies capable of targeting a wide range of CoVs to prevent severe disease following zoonotic outbreaks.

Coronaviruses encode for 16 highly conserved, non-structural proteins that are processed from two polyproteins, 1a and 1ab (pp1a and pp1ab) (1). The largest non-structural protein is non-structural protein 3 (nsp3) that encodes for multiple modular protein domains. Both the SARS-CoV and the SARS-CoV-2 nsp3 proteins include three tandem macrodomains, Mac1, Mac2, and Mac3 (2). Mac1 is present in all CoVs, unlike Mac2 and Mac3, and contains a conserved three-layered α/β/α fold, a common feature amongst all macrodomains. All CoV Mac1 proteins tested have mono-ADP-ribosylhydrolase (ARH) activity, though it remains unclear if they have significant poly-ARH activity (3-8). In contrast, Mac2 and Mac3 fail to bind ADP-ribose and instead bind to nucleic acids (9,10). Mac1 homologs are also found in alphaviruses, Hepatitis E virus, and Rubella virus, indicating that ADP-ribosylation may be a potent anti-viral post-translational modification (PTM) (11,12). All are members of the larger MacroD-type macrodomain family, which includes human macrodomains Mdo1 and Mdo2 (13).

ADP-ribosylation is a post-translational modification catalyzed by ADP-ribosyltransferases (ARTs, also known as PARPs) through transferring an ADP-ribose moiety

3

63   from NAD$^+$ onto target proteins or nucleic acids (14). ADP-ribose is transferred in as a single

64   unit as mono-ADP-ribose (MAR), or it is transferred consecutively and covalently attached

65   through glycosidic bonds to preceding ADP-ribose units to form a poly-ADP-ribose (PAR)

66   chain. Both mono- and poly-ARTs inhibit virus replication, implicating ADP-ribosylation in the

67   host-response to infection (15).

68   Several reports have addressed the role of Mac1 on the replication and pathogenesis of

69   CoVs, mostly using the mutation of a highly conserved asparagine to alanine (N41A-SARS-

70   CoV). This mutation abolished the MAR-hydrolase activity of SARS-CoV Mac1 (16). This

71   mutation has minimal effects on CoV replication in transformed cells, but reduces viral load,

72   leads to enhanced IFN production, and strongly attenuates both murine hepatitis virus (MHV)

73   and SARS-CoV in mouse models of infection (4,16-18). Murine hepatitis virus strain JHM

74   (MHV-JHM) Mac1 was also required for efficient replication in primary macrophages, which

75   could be partially rescued by the PARP inhibitors or siRNA knockdown of PARP12 or PARP14

76   (19). These data suggest that Mac1's function is to counter PARP-mediated anti-viral ADP-

77   ribosylation (20). More recently, we have identified mutations in the MHV-JHM Mac1 domain,

78   predicted to abolish ADP-ribose binding, that resulted in severe replication defects in cell

79   culture, indicating that for some CoVs Mac1 may be even more important than previously

80   appreciated (21). Mutations in the alphavirus and HEV macrodomain also have substantial

81   phenotypic effects on virus replication and pathogenesis (22-26).

82   As viral macrodomains are critical virulence factors, they are unique targets for anti-viral

83   therapeutics (20). Several studies have reported structures that could potentially bind to the ADP-

84   ribose binding pocket of SARS-CoV-2 Mac1. While most of these studies were limited to *in*

85   *silico* studies, a few have tested compound activity in biochemical assays, but have been met

86   with minimal success (27-30). The only compounds identified thus far that inhibit SARS-CoV-2

87   Mac1 with IC_{50} less than 100 μM are Suramin, which inhibited Mac1-ADP-ribose binding in a

88   FRET assay with an IC_{50} of 8.7 μM, and Dasatanib, which inhibited Mac1 mono-ARH activity

89   with an IC_{50} of ~50 μM. Suramin targeted several divergent macrodomains and is known to have

90   additional targets, and thus is not suitable for further evaluation (30). Dasatinib is not a candidate

91   for a Mac1 inhibitor as it is toxic to mammalian cells, though it may provide a scaffold for

92   further inhibitor development. None of the identified compounds have been tested for their

93   ability to inhibit Mac1 in cell culture or in animal models of disease.

94   Here, we optimized two high-throughput macrodomain-ADP-ribose binding assays, a

95   previously described luminescent-based AlphaScreen[TM] assay, and a novel fluorescence

96   polarization assay (31,32), and used the AlphaScreen[TM] assay to screen ~38,000 compounds for

97   their ability to inhibit SARS-CoV-2 Mac1-ADP-ribose binding. We identified 5 compounds

98   from 3 chemotypes that inhibited ADP-ribose binding by the SARS-CoV-2 Mac1 protein in both

99   assays, some with IC_{50} values as low as 5-10 μM. These compounds also demonstrated some

100   inhibition of ARH activity and have evidence of direct binding to Mac1. The profiling of the

101   most potent inhibitor against a panel of virus and human MAR binding and hydrolyzing proteins

102   revealed the remarkable selectivity of the inhibition of SARS-CoV-2 Mac1. These compounds

103   represent several series that can be further developed into potent Mac1 inhibitors and potential

104   therapeutics for SARS-CoV-2 and other CoVs of interest.

105

106   **RESULTS and DISCUSSION**

107   **Comparison of viral and human macrodomains in two high-throughput ADP-ribose**

108   **binding assays.** Here we established two distinct ADP-ribose binding assays for multiple

109   macrodomain proteins (Fig. 1A-C). First, we adopted a previously published AlphaScreen^{TM}

110   (AS) assay, where a short peptide was modified at a leucine residue with ADP-ribose through an

111   amino-oxyacetic acid linkage, and at a second leucine residue with biotin (Fig. 1A) (32).

112   Streptavidin donor beads and Ni^{2+} acceptor beads induce a light signal if the His-tagged Mac1

113   protein interacts with the biotinylated peptide (Fig. 1B). We also developed a fluorescent

114   polarization (FP) assay as an orthogonal assay to evaluate interactions of macrodomains with

115   ADP-ribosylated peptide. This assay used the same peptide but with fluorescein attached instead

116   of biotin and measures polarization of the fluorescent signal (Fig. 1C). We then tested 4 separate

117   macrodomains for their ability to bind to these peptides, the human macrodomain Mdo2, and

118   Mac1 from SARS-CoV, MERS-CoV, and SARS-CoV-2. All 4 macrodomains bound to the

119   ADP-ribosylated control peptides better than to non-ADP-ribosylated peptides (Fig. 1D,G). The

120   AS assay had an especially strong signal-to-background ratio, ranging from ~0.75-2×10^3. To

121   further study the binding of Mac1 proteins to AS and FP peptides, we evaluated binding in a

122   dose-dependent assay. Of these four proteins, the human MDO2 demonstrated the highest

123   affinity in both assays, with a K_D of 1.1 ± 0.3 µM in the FP assay and reached a maximum signal

124   in the AS assay at 40 nM (Fig. 1E,H). The SARS-CoV-2 Mac1 had a K_D of 3.4 ± 0.4 µM in the

125   FP assay and reached a maximum signal in the AS assay at 0.625 µM, while the SARS-CoV and

126   MERS-CoV Mac1 both reached their maximum signal in the AS assay at ~1.25-2.5 µM (AS)

127   and had K_D's of 7.7 ± 1.3 µM and 19.9 ± 3.3 µM in the FP assay, respectively (Fig. 1F,I).

128   Next, we tested the ability of free ADP-ribose to inhibit the binding of Mac1 to the ADP-

129   ribosylated peptide. For these displacement assays, the amount of beads, peptide, and Mac1

130   protein amounts to be used were optimized to obtain a robust signal while limiting the amount of

131   reagents used for screening purposes (see Methods). The addition of free ADP-ribose, but not

6

132   ATP, into the AS and FP assays inhibited human macrodomain and CoV Mac1 binding to the

133   ADP-ribosylated peptides, confirming that these assays can be used to identify macrodomain

134   binding inhibitors (Fig. 2). IC_{50} values for free ADP-ribose ranged between 0.24 µM with SARS-

135   CoV Mac1 to 1.5 µM with SARS-CoV-2 using the free ADP-ribose in the AS assay (Fig. 2A).

136   Similar results, albeit higher IC_{50} values were observed in the FP assay, likely because of higher

137   amount of Mac1 used in this assay (4 µM vs 250 nM), with IC_{50} values ranging from 2.3 µM to

138   9.74 µM (Fig. 2B).

139

140   **High-throughput screening (HTS) for SARS-CoV-2 Mac1 inhibitors.** We next performed a

141   small pilot screen of ~ 2,000 compounds from the Maybridge Mini Library of drug-like scaffolds

142   at 10 µM using both AS and FP assays (Fig. 3A-B). We identified 39 compounds that

143   significantly inhibited Mac1-ADP-ribose binding at >3 standard deviations (3SD) plus the plate

144   median (Fig. 3A-B). After performing dose-response curves we found that two compounds

145   inhibited binding in both assays (Fig. 4A). We then tested these compounds in a counter screen,

146   which is also an AS assay that utilizes a biotinylated-His peptide that gives off a strong signal

147   with the addition of streptavidin donor and nickel acceptor beads. These two compounds did not

148   affect the signal from our counter screen indicating that they do not intrinsically inhibit the assay.

149   After this initial validation of our screen, three additional libraries were chosen to include a total

150   number of 35,863 compounds from the Analyticon, 3D BioDiversity, and Peptidomimetics

151   libraries (Fig. 3A). We chose the AS assay as our primary HTS assay, as the average Z' score for

152   the AS was higher than the Z' score from the FP assay in our original screen (0.82 vs 0.67). In

153   this larger screen, the average Z' was 0.89±0.05, indicating a strong separation between positive

154   and negative controls (Fig. 3C). Using the same hit criteria described above for each individual

7

155   library, we identified 406 hits resulting in a 1% hit rate (Fig. 3D). Of note, the Analyticon library

156   produced a lot of non-specific inhibitors, indicating a lot of these compounds likely inhibit the

157   assays themselves (Fig. 3B). We next performed dose-response (10-40 μM) curves of these 406

158   compounds in our primary (AS), orthogonal (FP), and counter screen (Bn-His$_6$) assays (Fig. 3).

159   From the 406 original hits, 26 compounds were identified that inhibited SARS-CoV-2 Mac1-

160   ADP-ribose binding in the AS assay in a dose-dependent fashion, and 6 compounds were

161   identified that inhibited Mac1 binding in both AS and FP assays (Fig. 3D). Of these 32 hit

162   compounds, we re-purchased 17 of them, excluding 15 based on several selection criteria,

163   including substantial inhibition of the counter screen, high IC$_{50}$ values in the AlphaScreen, pan-

164   assay interference compounds, and compound availability (Fig. 3D). The remaining 17

165   compounds along with 4 analogs were repurchased or resynthesized (see Methods).

166   Re-purchased compounds were evaluated in dose-response assays against both SARS-

167   CoV-2 Mac1 and human MDO2 protein. Our cutoff criteria included: *i)* compound must inhibit

168   both primary and orthogonal assays with at least 75% inhibition in AS assay and at or near 50%

169   inhibition in the FP assay, and *ii)* less than 30% inhibition of the Bn-His$_6$ counter screen. Among

170   the 17 selected and the 4 analogs compounds, six compounds inhibited ADP-ribose binding of

171   SARS-CoV-2 Mac1 in both AS and FP assays with no substantial inhibition of the Bn-His$_6$

172   counter screen. These were compounds **1,2,6,7,10**, and **11** (Table 1). IC$_{50}$ values ranged from 6.2

173   μM to 112.2 μM in AS assay and 7.3 μM to 159.4 μM in FP assay (Table 1, Fig. 4). Compounds

174   **1**, **10**, and **11** also had some inhibitory activity against the MERS-CoV Mac1 protein, though the

175   inhibition of MERS-CoV Mac1 was lower than the inhibition demonstrated against SARS-CoV-

176   2 (Table 1). In addition, only compound **2** inhibited MDO2, indicating that these compounds

177   were broadly specific for viral macrodomains.

8

178

179   **Selected compounds demonstrate evidence of SARS-CoV-2 Mac 1 binding.** Next, we set out

180   to test the hypothesis that these compounds inhibit Mac1-ADP-ribose by binding to Mac1, and

181   not other components of the assay, such as the peptide. To test for Mac1 binding, we used a

182   differential scanning fluorimetry (DSF) assay as previously described (8) and tested our top 6 hit

183   compounds (Fig. 5, S1) and compounds **8** and **9**, as they are analogs of **6** and **7** (Fig. S2). In this

184   assay, compound binding to Mac1 should increase the melting temperature of Mac1. The

185   addition of free ADP-ribose, which binds to Mac1, showed a dose-dependent increase of

186   approximately 4°C in the melting temperature of Mac1, while the negative control, ATP, had no

187   effect, as previously demonstrated (8). **1**, **6**, **7**, **10**, and **11** showed dose-dependent shifts in the

188   melting temperature of Mac1 ranging from 0.2 - 1.5°C, providing strong evidence that these

189   compounds bind to Mac1, albeit not with the same affinity as ADP-ribose. On the other hand,

190   compound **2** resulted in highly irregular thermal shift curves, indicating that this compound may

191   not be a true Mac1 binder (Fig. 5, S1). These results provide evidence that 5 of our 6 hit

192   compounds (**1**, **6**, **7**, **10**, and **11**) directly bind to SARS-CoV-2 Mac1.

193

194   **Hit compounds inhibit ADP-ribosylhydrolase activity *in vitro*.** SARS-CoV-2 Mac1 is a

195   mono-ADP-ribosylhydrolase that removes mono-ADP-ribose from target proteins (8). Next, we

196   examined the ability of some of our top 5 hit compounds to inhibit the enzymatic activity of

197   SARS-CoV-2 Mac1 using two distinct assays. The first approach was a gel-based Mac1 ADP-

198   ribosylhydrolase assay where we tested each compound against the SARS-CoV-2 Mac1 protein

199   (8). Compound **1** tended to precipitate in these assays at higher concentrations, and so we used

200   lower concentrations for this compound than others. Compounds **1**, **6,** and **7** exhibited a dose-

9

201   dependent inhibition of Mac1 ADP-ribosylhydrolase activity (Fig. 6A). We were unable to detect

202   any significant inhibition with **10** and **11** in this assay.

203   Next, we utilized a recently published high-throughput luminescence-based ADP-

204   ribosylhydrolyase assay (33). Here we found that **1**, **6**, **7**, **10** and **11** all showed dose-dependent

205   inhibition of ADP-ribosylhydrolase activity (Fig. 6B). **6** was clearly the most efficient inhibitor,

206   as it had a peak of ~60% inhibition, similar to Dasatinib which we previously identified in a

207   separate HTS (33). In contrast to the gel-based assay, **10** and **11** did inhibit ADP-

208   ribosylhydrolase activity in this assay, likely reflecting the increased sensitivity of this assay

209   compared to the gel-based assay. These results indicate that the identified Mac1 inhibitors block

210   Mac1 binding and Mac1 enzymatic activity.

211

212   **Selectivity Profiling.** As compound **6** inhibited both Mac1 ADP-ribose binding and hydrolysis

213   activity, and showed the strongest evidence of direct Mac1 binding, we tested its ability to inhibit

214   16 different macrodomains using a recently developed FRET-based assay (30). Again, **6**

215   demonstrated dose-dependent inhibition of Mac1-ADP-ribose binding in this assay, consistent

216   with our AS results but with a slightly higher IC_{50} of 45.0 ± 10.9 µM (Fig. 7A). Remarkably,

217   when tested again 16 different human and viral macrodomains in this assay, **6** only inhibited

218   SARS-CoV-2 Mac1, having only minimal levels in inhibition of all other macrodomain proteins,

219   including other CoV macrodomains (Fig. 7B), which is in agreement with the selectivity

220   observed in AS (Table 1). These results indicate that this compound is highly selective for the

221   SARS-CoV-2 Mac1 protein.

222

223   **Structure activity relationship (SAR).** The top 5 compounds could be separated into 3

224   chemotypes based on their structures. To analyze the involved residues and type of connection

225   between selected hit compound and Mac1, we used computational docking analysis to get an

226   initial structure activity relationship (SAR) by predicting poses of compounds in Mac1

227   structures. In addition to our 5 hit compounds, we also docked compounds **8** and **9** as they are

228   analogs of **6** and **7** and could give further insight into SAR, even though we either detected

229   minimal or no direct Mac1 binding by these compounds. These seven compounds were docked

230   against the ADP-ribose bound structure of SARS-CoV-2 Mac1 (PDB 6WOJ) as well as three apo

231   structures of Mac1 were used (PDB 7KR0, 7KR1, 6WEY). Docking and glide emodel scores

232   were calculated for each compound against all four structures and the best structure was chosen

233   based on these scores (Table S1). Analog compounds **6**, **7**, **8**, and **9** were assessed both based on

234   score and visual inspection, and were re-docked using a core constraint to a high scoring,

235   intuitive pose of compound **7**. All top scoring poses were subsequently minimized using Prime,

236   allowing flexibility within 5 Å of the ligand. Compound **1** was its own chemotype but has a

237   sulfonohydrazide that is also found in a compound identified in a previous screen for Mac1

238   compounds (34). It also has a thienopyrimidine that is similar to the pyrrolopyrimidine found in

239   of the compounds identified in the fragment screen by Schuller et al (31). It makes a hydrogen

240   bond with a backbone amine of D22, pie-stacking interactions with F156, and extends with a

241   benzene ring into the distal ribose pocket inserting in between the GGG and GIF loops (Fig. 8A).

242   Compounds **10** and **11** are close analogs with a single difference of positioning in the

243   bromobenzoyl moiety on the piperidine ring (Fig. 4C). These compounds had similar activity

244   across the board in our assays, making it difficult to analyze their SAR. While they docked into

245   the binding pocket, these docking poses only indicate a single hydrogen bond with the backbone

11

246   amino of D22. In contrast, compounds **6**, **7**, **8**, and **9** are close analogs of each other and have a

247   wide-range of inhibitory and binding activity. IC_{50} values for these compounds range from 10 to

248   several hundred μM (Table 1). Direct binding also varied substantially, with T_m's ranging from

249   ~1.7 °C (**6**) to undetectable binding (**8**). These compounds all have the same base structure,

250   including a beta-alanine core substituted with a N-benzyl or N-chlorobenzyl group, a methoxy

251   benzoyl group and a piperazine amide. The main difference between **6** and its analogs are the

252   addition of a methoxy group on the benzoyl group (**7**), the loss of a chlorine (**8**), and a missing

253   methoxy group (**9**). Each of these changes reduces the activity of this series indicating that *i)* the

254   orientation of the methoxy groups on **6** is likely important for its increased activity, *ii)*

255   reorienting **7** to accommodate the 4-methoxy group likely decreases activity due to the disruption

256   of multiple interactions, and *iii)* the chlorine likely makes a critical halogen bond with a

257   backbone amino group of L126 in the binding pocket.

258   In conclusion, we developed multiple high-throughput ADP-ribose binding assays and

259   performed HTS to identify high-quality Mac1 inhibitors. We followed these screens with several

260   additional assays to measure their ability to inhibit ADP-ribosylhydrolase activity and their direct

261   binding to Mac1. We have identified 5 compounds that inhibit both the primary and orthogonal

262   assays without inhibiting the counter screen and demonstrate dose-dependent inhibition of Mac1

263   enzymatic activity. Compounds **1** and **6** are particularly effective with IC_{50} values of ~10 μM in

264   the AS assay, along with thermal shifts and docking poses that indicate direct binding to Mac1.

265   Compound **6** shows excellent selectivity towards SARS-CoV-2 over the human macrodomains

266   guiding further development of the compound. We expect that these compounds could be

267   utilized for further derivatization and optimization into more potent Mac1 inhibitors.

12

268 **METHODS**

269 **Reagents**

270   All plasmids and proteins used were expressed and purified as previously described

271 (30,35-37). All compounds were repurchased from MolPort except for compounds **6** and **10**,

272 which were repurchased from ChemDiv. After reordering once, compounds **10** and **11** became

273 unavailable and thus were resynthesized according to the literature (38). ADP-ribosylated

274 peptides were purchased from Cambridge peptides.

275 **Differential Scanning Fluorimetry (DSF)**

276   Thermal shift assay with DSF involved use of LightCycler® 480 Instrument (Roche

277 Diagnostics). In total, a 15 μL mixture containing 8X SYPRO Orange (Invitrogen), and 10 μM

278 macrodomain protein in buffer containing 20 mM HEPES, NaOH, pH 7.5 and various

279 concentrations of ADP-ribose or hit compounds were mixed on ice in 384-well PCR plate

280 (Roche). Fluorescent signals were measured from 25 to 95 °C in 0.2 °C/30/Sec steps (excitation,

281 470-505 nm; detection, 540-700 nm). The main measurements were carried out in triplicate. Data

282 evaluation and T_m determination involved use of the Roche LightCycler® 480 Protein Melting

283 Analysis software, and data fitting calculations involved the use of single site binding curve

284 analysis on GraphPad Prism. The thermal shift (ΔT_m) was calculated by subtracting the T_m

285 values of the DMSO from the T_m values of compounds.

286 **AlphaScreen (AS) Assay**

287   The AlphaScreen reactions were carried out in 384-well plates (Alphaplate, PerkinElmer,

288 Waltham, MA) in a total volume of 40 μL in buffer containing 25 mM HEPES (pH 7.4), 100

289 mM NaCl, 0.5 mM TCEP, 0.1% BSA, and 0.05% CHAPS. All reagents were prepared as 4X

290 stocks and 10 μL volume of each reagent was added to a final volume of 40 μL. All compounds

13

291 were transferred acoustically using ECHO 555 (Beckman Inc) and preincubated after mixing

292 with purified His-tagged macrodomain protein (250 nM) for 30 min at RT, followed by addition

293 of a 10 amino acid biotinylated and ADP-ribosylated peptide [ARTK(Bio)QTARK(Aoa-

294 RADP)S] (Cambridge peptides) (625 nM). After 1h incubation at RT, streptavidin-coated donor

295 beads (7.5 μg/mL) and nickel chelate acceptor beads (7.5 μg/mL); (PerkinElmer AlphaScreen

296 Histidine Detection Kit) were added under low light conditions, and plates were shaken at 400

297 rpm for 60 min at RT protected from light. Plates were kept covered and protected from light at

298 all steps and read on BioTek plate reader using an AlphaScreen 680 excitation/570 emission

299 filter set. For counter screening of the compounds, 25 nM biotinylated and hexahistidine-tagged

300 linker peptide (Bn-His$_6$) (PerkinElmer) was added to the compounds, followed by addition of

301 beads as described above.

Fluorescence Polarization (FP) Assay

303 The FP assay was performed in buffer containing 25 mM Tris pH7.5, NaCl 50 mM,

304 0.025% TritonX-100. All reagents were prepared as 2X stocks and 10 μL volume of each reagent

305 was added to a final volume of 20 μL. Compounds were preincubated with His-Macrodomain

306 proteins (4 μM) for 30', RT in black 384 well plates (Corning 3575 plates), followed by addition

307 of 50 nM of fluorescein labeled ADP-ribosylated peptide [5Flu-ARTKQTARK(Aoa-RADP)S].

308 After mixing for a minute, the plate was incubated at 25°C, protected from light and fluorescence

309 polarization was read after 30 minutes, 1h and 2h using a plate reader.

Gel-based Inhibition of Mono-ADP-ribosylhydrolase activity (de-MARylaion)

311 PARP10-CD protein was auto-MARylated through incubation for 20 minutes at 37°C

312 with 1 mM final concentration of β-Nicotinamide Adenine Dinucleotide (β NAD$^+$) (Millipore-

313 Sigma) in a reaction buffer (50 mM HEPES, 150 mM NaCl, 0.2 mM DTT, and 0.02% NP-40).

314   MARylated PARP10 was aliquoted and stored at -80°C. To test the ability of identified

315   compounds for their ability to inhibit MARylation activity of Mac1, we first incubated each

316   compound with purified SARS-CoV-2 Mac1 in the reaction buffer (50 mM HEPES, 150 mM

317   NaCl, 0.2 mM DTT, and 0.02% NP-40) at 37°C for 30 min. Then, MARylated PARP10-CD was

318   added to this mixture solution and further incubated for 30 min at 37°C. The reaction was

319   stopped with addition of 2X Laemmli sample buffer containing 10% β-mercaptoethanol. Protein

320   samples were heated at 95°C for 5 minutes before loading and separated onto SDS-PAGE

321   cassette (Thermo Fisher Scientific Bolt™ 4-12% Bis-Tris Plus Gels) in MES running buffer. For

322   immunoblotting, the separated proteins were transferred onto polyvinylidene difluoride (PVDF)

323   membrane using iBlot™ 2 Dry Blotting System (ThermoFisher Scientific). The blot was blocked

324   with 5% skim milk in 1xPBS and probed with the anti-mono-ADP-ribose binding

325   reagent/antibody MABE1076 (α-MAR), and anti-GST tag monoclonal antibody MA4-004

326   (ThermoFisher Scientific). The primary antibodies were detected with secondary anti-rabbit and

327   anti-mouse antibodies (LI-COR Biosciences). All immunoblots were visualized using

328   Odyssey® CLx Imaging System (LI-COR Biosciences). The images were quantitated using the

329   LI-COR Image Studio software.

330   **ADP-ribosylhydrolase assay**

331   The recently published assay, ADPr-Glo, was used to examine the impact of our top hit

332   compounds on SARS-CoV-2 enzymatic activity (33). Briefly, the compounds were preincubated

333   with SARS-CoV-2 Mac1 (2 nM) and NudF (125 nM) at ambient temperature for 30 min prior to

334   the addition of MARylated PARP-10 derived substrate. The substrate (20 µM) was then

335   incubated with the SARS-CoV-2 Mac1 and NudF at ambient temperature for 30 min. The

336   reaction products were measured with AMP-Glo. Reactions without macrodomains were

15

337   performed in parallel as a negative control. Luminescence signal was converted to AMP

338   concentration via interpolation from an AMP standard curve. Data plotted are AMP generated by

339   the macrodomain and NudF, subtracted by AMP generated from NudF alone. Inhibition

340   percentages were calculated and non-linear regression analysis was performed in GraphPad

341   Prism.

A FRET based binding assay and inhibitor profiling

343   FRET method was utilized for the profiling of MCD-628 a panel of human and viral

344   macrodomains to determine their specificity (30,36). The assay is based on the site-specific

345   introduction of cysteine-linked mono-ADP-ribose to the C-terminal Gαi peptide (GAP) by

346   Pertussis toxin subunit1 (PtxS1) fused to YFP. To generate the FRET signal ADP-ribosyl binders

347   were fused to CFP. Samples were prepared in the assay buffer (for most binders; 10 mM Bis-

348   Tris propane pH 7.0, 3 % (w/v) PEG 20,000, 0.01 % (v/v) Triton X-100 and 0.5 mM TCEP), (for

349   TARG1; 10 mM Bis-Tris propane pH 7.0, 150 mM NaCl, 0.01 % (v/v) Triton X-100 and 0.5

350   mM TCEP), (for PARG; 10 mM Bis-Tris propane pH 7.0, 25 mM NaCl, 0.01 % (v/v) Triton X-

351   100 and 0.5 mM TCEP) in a 384-well black polypropylene flat-bottom plates (Greiner, Bio-one)

352   with 10 µL reaction volume per well. The reactions consisted of 1 µM CFP-fused binders and 5

353   µM MARylated YFP-GAP. Reactions were excited at 410 nm (20 nm bandwidth), while the

354   emission signal was measured at 477 nm (10 nm bandwidth) and 527 nm (10 nm bandwidth).

355   Afterwards, blank was deducted from the individual values and the radiometric FRET (rFRET)

356   was calculated by dividing the fluorescence intensities at 527 nm by 477 nm. Compound was

357   dispensed with Echo acoustic liquid dispenser (Labcyte, Sunnyvate, CA). Dispensing of larger

358   volumes of the solutions was carried out by using Microfluidic Liquid Handler (MANTIS®,

16

359   Formulatrix, Beford, MA, USA). Measurements were taken with Tecan Infinite M1000 pro plate

360   reader.

361   **Computational modeling**

362   Hit compounds were docked into the ADPr-bound (6WOJ), 3 unique unbound

363   conformations (7KR0, 7KR1, 6WEY) and two small molecule bound (5RSG, 5RTT) structures

364   of SARS-CoV-2 Mac1 (35,39,40). The proteins and ligands were prepared using Schrodinger

365   Maestro and were subsequently docked using Glide with XP precision, analog compounds **6**, **7**,

366   **8**, and **9** were re-docked using a core constraint to a high scoring, intuitive pose of compound **7,**

367   and high scoring poses were subjected to a Prime MM-GBSA minimization, allowing flexibility

368   for any residue within 5 Å of the ligand (41-46).

ACKNOWLEDGEMENTS

REFERENCES

1. Fehr, A. R., and Perlman, S. (2015) Coronaviruses: An Overview of Their Replication and Pathogenesis. in *Coronaviruses* (Maier, H. J., Bickerton, E., and Britton, P. eds.), Springer New York. pp 1-23

2. Srinivasan, S., Cui, H., Gao, Z., Liu, M., Lu, S., Mkandawire, W., Narykov, O., Sun, M., and Korkin, D. (2020) Structural Genomics of SARS-CoV-2 Indicates Evolutionary Conserved Functional Regions of Viral Proteins. *Viruses* **12**, 360

3. Egloff, M. P., Malet, H., Putics, A., Heinonen, M., Dutartre, H., Frangeul, A., Gruez, A., Campanacci, V., Cambillau, C., Ziebuhr, J., Ahola, T., and Canard, B. (2006) Structural and functional basis for ADP-ribose and poly(ADP-ribose) binding by viral macro domains. *J Virol* **80**, 8493-8502

4. Putics, A., Filipowicz, W., Hall, J., Gorbalenya, A. E., and Ziebuhr, J. (2005) ADP-ribose-1"-monophosphatase: a conserved coronavirus enzyme that is dispensable for viral replication in tissue culture. *J Virol* **79**, 12721-12731

5. Saikatendu, K. S., Joseph, J. S., Subramanian, V., Clayton, T., Griffith, M., Moy, K., Velasquez, J., Neuman, B. W., Buchmeier, M. J., Stevens, R. C., and Kuhn, P. (2005) Structural basis of severe acute respiratory syndrome coronavirus ADP-ribose-1"-phosphate dephosphorylation by a conserved domain of nsP3. *Structure* **13**, 1665-1675

6. Cho, C. C., Lin, M. H., Chuang, C. Y., and Hsu, C. H. (2016) Macro Domain from Middle East Respiratory Syndrome Coronavirus (MERS-CoV) Is an Efficient ADP-ribose Binding Module: CRYSTAL STRUCTURE AND BIOCHEMICAL STUDIES. *J Biol Chem* **291**, 4894-4902

7. Xu, Y. Y., Cong, L., Chen, C., Wei, L., Zhao, Q., Xu, X. L., Ma, Y. L., Bartlam, M., and Rao, Z. H. (2009) Crystal Structures of Two Coronavirus ADP-Ribose-1 "-Monophosphatases and Their Complexes with ADP-Ribose: a Systematic Structural Analysis of the Viral ADRP Domain. *Journal of Virology* **83**, 1083-1092

8. Alhammad, Y. M. O., Kashipathy, M. M., Roy, A., Gagne, J. P., McDonald, P., Gao, P., Nonfoux, L., Battaile, K. P., Johnson, D. K., Holmstrom, E. D., Poirier, G. G., Lovell, S., and Fehr, A. R. (2021) The SARS-CoV-2 Conserved Macrodomain Is a Mono-ADP-Ribosylhydrolase. *J. Virol.* **95**, e01969-01920

9. Tan, J., Vonrhein, C., Smart, O. S., Bricogne, G., Bollati, M., Kusov, Y., Hansen, G., Mesters, J. R., Schmidt, C. L., and Hilgenfeld, R. (2009) The SARS-Unique Domain (SUD) of SARS Coronavirus Contains Two Macrodomains That Bind G-Quadruplexes. *PLoS Path.* **5**, e1000428

10. Chatterjee, A., Johnson, M. A., Serrano, P., Pedrini, B., Joseph, J. S., Neuman, B. W., Saikatendu, K., Buchmeier, M. J., Kuhn, P., and Wüthrich, K. (2009) Nuclear magnetic resonance structure shows that the severe acute respiratory syndrome coronavirus-unique domain contains a macrodomain fold. *Journal of virology* **83**, 1823-1836

11. Makrynitsa, G. I., Ntonti, D., Marousis, K. D., Birkou, M., Matsoukas, M. T., Asami, S., Bentrop, D., Papageorgiou, N., Canard, B., Coutard, B., and Spyroulias, G. A. (2019) Conformational plasticity of the VEEV macro domain is important for binding of ADP-ribose. *J Struct Biol* **206**, 119-127

12. Malet, H., Coutard, B., Jamal, S., Dutartre, H., Papageorgiou, N., Neuvonen, M., Ahola, T., Forrester, N., Gould, E. A., Lafitte, D., Ferron, F., Lescar, J., Gorbalenya, A. E., de Lamballerie, X., and Canard, B. (2009) The crystal structures of Chikungunya and

428   Venezuelan equine encephalitis virus nsP3 macro domains define a conserved adenosine
429   binding pocket. *J Virol* **83**, 6534-6545

430 13. Rack, J. G., Perina, D., and Ahel, I. (2016) Macrodomains: Structure, Function,
431   Evolution, and Catalytic Activities. *Annu Rev Biochem* **85**, 431-454

432 14. Kim, D. S., Challa, S., Jones, A., and Kraus, W. L. (2020) PARPs and ADP-ribosylation
433   in RNA biology: from RNA expression and processing to protein translation and
434   proteostasis. *Genes Dev.* **34**, 302-320

435 15. Fehr, A. R., Singh, S. A., Kerr, C. M., Mukai, S., Higashi, H., and Aikawa, M. (2020)
436   The impact of PARPs and ADP-ribosylation on inflammation and host-pathogen
437   interactions. *Genes Dev* **34**, 341-359

438 16. Fehr, A. R., Channappanavar, R., Jankevicius, G., Fett, C., Zhao, J., Athmer, J.,
439   Meyerholz, D. K., Ahel, I., and Perlman, S. (2016) The Conserved Coronavirus
440   Macrodomain Promotes Virulence and Suppresses the Innate Immune Response during
441   Severe Acute Respiratory Syndrome Coronavirus Infection. *mBio* **7**, e01721-01716

442 17. Eriksson, K. K., Cervantes-Barragan, L., Ludewig, B., and Thiel, V. (2008) Mouse
443   hepatitis virus liver pathology is dependent on ADP-ribose-1"-phosphatase, a viral
444   function conserved in the alpha-like supergroup. *J Virol* **82**, 12325-12334

445 18. Fehr, A. R., Athmer, J., Channappanavar, R., Phillips, J. M., Meyerholz, D. K., and
446   Perlman, S. (2015) The nsp3 macrodomain promotes virulence in mice with coronavirus-
447   induced encephalitis. *J Virol* **89**, 1523-1536

448 19. Grunewald, M. E., Chen, Y., Kuny, C., Maejima, T., Lease, R., Ferraris, D., Aikawa, M.,
449   Sullivan, C. S., Perlman, S., and Fehr, A. R. (2019) The coronavirus macrodomain is
450   required to prevent PARP-mediated inhibition of virus replication and enhancement of
451   IFN expression. *PLoS Pathog* **15**, e1007756

452 20. Alhammad, Y. M. O., and Fehr, A. R. (2020) The Viral Macrodomain Counters Host
453   Antiviral ADP-Ribosylation. *Viruses* **12**, 384

454 21. Voth, L. S., O'Connor, J. J., Kerr, C. M., Doerger, E., Schwarting, N., Sperstad, P.,
455   Johnson, D. K., and Fehr, A. R. (2021) Unique mutations in the MHV macrodomain
456   differentially attenuate virus replication, indicating multiple roles for the macrodomain in
457   coronavirus replication. *Journal of Virology*, JVI. 00766-00721

458 22. Abraham, R., Hauer, D., McPherson, R. L., Utt, A., Kirby, I. T., Cohen, M. S., Merits,
459   A., Leung, A. K. L., and Griffin, D. E. (2018) ADP-ribosyl-binding and hydrolase
460   activities of the alphavirus nsP3 macrodomain are critical for initiation of virus
461   replication. *Proc Natl Acad Sci U S A* **115**, E10457-E10466

462 23. Abraham, R., McPherson, R. L., Dasovich, M., Badiee, M., Leung, A. K. L., and Griffin,
463   D. E. (2020) Both ADP-Ribosyl-Binding and Hydrolase Activities of the Alphavirus
464   nsP3 Macrodomain Affect Neurovirulence in Mice. *mBio* **11**

465 24. McPherson, R. L., Abraham, R., Sreekumar, E., Ong, S. E., Cheng, S. J., Baxter, V. K.,
466   Kistemaker, H. A., Filippov, D. V., Griffin, D. E., and Leung, A. K. (2017) ADP-
467   ribosylhydrolase activity of Chikungunya virus macrodomain is critical for virus
468   replication and virulence. *Proc Natl Acad Sci U S A* **114**, 1666-1671

469 25. Li, C., Debing, Y., Jankevicius, G., Neyts, J., Ahel, I., Coutard, B., and Canard, B. (2016)
470   Viral Macro Domains Reverse Protein ADP-Ribosylation. *J Virol* **90**, 8478-8486

471 26. Parvez, M. K. (2015) The hepatitis E virus ORF1 'X-domain' residues form a putative
472   macrodomain protein/Appr-1"-pase catalytic-site, critical for viral RNA replication. *Gene*
473   **566**, 47-53

27. Schuller, M., Correy, G. J., Gahbauer, S., Fearon, D., Wu, T., Díaz, R. E., Young, I. D., Martins, L. C., Smith, D. H., and Schulze-Gahmen, U. (2021) Fragment binding to the Nsp3 macrodomain of SARS-CoV-2 identified through crystallographic screening and computational docking. *Science advances* **7**, eabf8711

28. Virdi, R. S., Bavisotto, R. V., Hopper, N. C., Vuksanovic, N., Melkonian, T. R., Silvaggi, N. R., and Frick, D. N. (2020) Discovery of drug-like ligands for the Mac1 domain of SARS-CoV-2 Nsp3. *SLAS DISCOVERY: Advancing the Science of Drug Discovery* **25**, 1162-1170

29. Russo, L. C., Tomasin, R., Matos, I. A., Manucci, A. C., Sowa, S. T., Dale, K., Caldecott, K. W., Lehtiö, L., Schechtman, D., and Meotti, F. C. (2021) The SARS-CoV-2 Nsp3 macrodomain reverses PARP9/DTX3L-dependent ADP-ribosylation induced by interferon signalling. *bioRxiv*

30. Sowa, S. T., Galera-Prat, A., Wazir, S., Alanen, H. I., Maksimainen, M. M., and Lehtio, L. (2021) A molecular toolbox for ADP-ribosyl binding proteins. *Cell Rep Methods*, 100121

31. Schuller, M., Correy, G. J., Gahbauer, S., Fearon, D., Wu, T., Diaz, R. E., Young, I. D., Carvalho Martins, L., Smith, D. H., Schulze-Gahmen, U., Owens, T. W., Deshpande, I., Merz, G. E., Thwin, A. C., Biel, J. T., Peters, J. K., Moritz, M., Herrera, N., Kratochvil, H. T., Consortium, Q. S. B., Aimon, A., Bennett, J. M., Brandao Neto, J., Cohen, A. E., Dias, A., Douangamath, A., Dunnett, L., Fedorov, O., Ferla, M. P., Fuchs, M. R., Gorrie-Stone, T. J., Holton, J. M., Johnson, M. G., Krojer, T., Meigs, G., Powell, A. J., Rack, J. G. M., Rangel, V. L., Russi, S., Skyner, R. E., Smith, C. A., Soares, A. S., Wierman, J. L., Zhu, K., O'Brien, P., Jura, N., Ashworth, A., Irwin, J. J., Thompson, M. C., Gestwicki, J. E., von Delft, F., Shoichet, B. K., Fraser, J. S., and Ahel, I. (2021) Fragment binding to the Nsp3 macrodomain of SARS-CoV-2 identified through crystallographic screening and computational docking. *Sci Adv* **7**, eabf8711

32. Schuller, M., Riedel, K., Gibbs-Seymour, I., Uth, K., Sieg, C., Gehring, A. P., Ahel, I., Bracher, F., Kessler, B. M., Elkins, J. M., and Knapp, S. (2017) Discovery of a Selective Allosteric Inhibitor Targeting Macrodomain 2 of Polyadenosine-Diphosphate-Ribose Polymerase 14. *ACS Chem Biol* **12**, 2866-2874

33. Dasovich, M., Zhuo, J., Goodman, J. A., Thomas, A., McPherson, R. L., Jayabalan, A. K., Busa, V. F., Cheng, S. J., Murphy, B. A., Redinger, K. R., Alhammad, Y. M. O., Fehr, A. R., Tsukamoto, T., Slusher, B. S., Bosch, J., Wei, H., and Leung, A. K. L. (2022) High-Throughput Activity Assay for Screening Inhibitors of the SARS-CoV-2 Mac1 Macrodomain. *ACS Chem Biol* **17**, 17-23

34. Ekblad, T., Verheugd, P., Lindgren, A. E., Nyman, T., Elofsson, M., and Schuler, H. (2018) Identification of Poly(ADP-Ribose) Polymerase Macrodomain Inhibitors Using an AlphaScreen Protocol. *SLAS Discov* **23**, 353-362

35. Alhammad, Y. M. O., Kashipathy, M. M., Roy, A., Gagne, J. P., McDonald, P., Gao, P., Nonfoux, L., Battaile, K. P., Johnson, D. K., Holmstrom, E. D., Poirier, G. G., Lovell, S., and Fehr, A. R. (2021) The SARS-CoV-2 Conserved Macrodomain Is a Mono-ADP-Ribosylhydrolase. *J Virol* **95**

36. Sowa, S. T., Galera-Prat, A., Wazir, S., Alanen, H. I., Maksimainen, M. M., and Lehtio, L. (2022) Preparation of screening assays for ADP-ribosyl readers and erasers using the GAP-tag as a binding probe. *STAR Protoc* **3**, 101147

37. Dasovich, M., Zhuo, J., Goodman, J. A., Thomas, A. G., McPherson, R. L., Jayabalan, A. K., Busa, V. F., Cheng, S. J., Murphy, B. A., Redinger, K. R., Alhammad, Y. M. O., Fehr, A. R., Tsukamoto, T., Slusher, B., Bosch, J., Wei, H., and Leung, A. K. L. (2022) High-throughput Activity Assay for Screening Inhibitors of the SARS-CoV-2 Mac1 Macrodomain. *ACS Chem Biol*

38. Capobianco, A. J., Schürer, S. C., Zhu, X., and Kelley, T. T. (2021) Inhibitors of the notch transcriptional activation complex kinase (" nack") and methods for use of the same. Google Patents

39. Frick, D. N., Virdi, R. S., Vuksanovic, N., Dahal, N., and Silvaggi, N. R. (2020) Molecular Basis for ADP-Ribose Binding to the Mac1 Domain of SARS-CoV-2 nsp3. *Biochemistry* **59**, 2608-2615

40. Schuller, M., Correy, G. J., Gahbauer, S., Fearon, D., Wu, T., Diaz, R. E., Young, I. D., Carvalho Martins, L., Smith, D. H., Schulze-Gahmen, U., Owens, T. W., Deshpande, I., Merz, G. E., Thwin, A. C., Biel, J. T., Peters, J. K., Moritz, M., Herrera, N., Kratochvil, H. T., Consortium, Q. S. B., Aimon, A., Bennett, J. M., Brandao Neto, J., Cohen, A. E., Dias, A., Douangamath, A., Dunnett, L., Fedorov, O., Ferla, M. P., Fuchs, M. R., Gorrie-Stone, T. J., Holton, J. M., Johnson, M. G., Krojer, T., Meigs, G., Powell, A. J., Rack, J. G. M., Rangel, V. L., Russi, S., Skyner, R. E., Smith, C. A., Soares, A. S., Wierman, J. L., Zhu, K., O'Brien, P., Jura, N., Ashworth, A., Irwin, J. J., Thompson, M. C., Gestwicki, J. E., von Delft, F., Shoichet, B. K., Fraser, J. S., and Ahel, I. (2021) Fragment binding to the Nsp3 macrodomain of SARS-CoV-2 identified through crystallographic screening and computational docking. *Sci Adv* **7**

41. Friesner, R. A., Banks, J. L., Murphy, R. B., Halgren, T. A., Klicic, J. J., Mainz, D. T., Repasky, M. P., Knoll, E. H., Shelley, M., Perry, J. K., Shaw, D. E., Francis, P., and Shenkin, P. S. (2004) Glide: a new approach for rapid, accurate docking and scoring. 1. Method and assessment of docking accuracy. *J Med Chem* **47**, 1739-1749

42. Friesner, R. A., Murphy, R. B., Repasky, M. P., Frye, L. L., Greenwood, J. R., Halgren, T. A., Sanschagrin, P. C., and Mainz, D. T. (2006) Extra precision glide: docking and scoring incorporating a model of hydrophobic enclosure for protein-ligand complexes. *J Med Chem* **49**, 6177-6196

43. Halgren, T. A., Murphy, R. B., Friesner, R. A., Beard, H. S., Frye, L. L., Pollard, W. T., and Banks, J. L. (2004) Glide: a new approach for rapid, accurate docking and scoring. 2. Enrichment factors in database screening. *J Med Chem* **47**, 1750-1759

44. Jacobson, M. P., Friesner, R. A., Xiang, Z., and Honig, B. (2002) On the role of the crystal environment in determining protein side-chain conformations. *J Mol Biol* **320**, 597-608

45. Jacobson, M. P., Pincus, D. L., Rapp, C. S., Day, T. J., Honig, B., Shaw, D. E., and Friesner, R. A. (2004) A hierarchical approach to all-atom protein loop prediction. *Proteins* **55**, 351-367

46. Sastry, G. M., Adzhigirey, M., Day, T., Annabhimoju, R., and Sherman, W. (2013) Protein and ligand preparation: parameters, protocols, and influence on virtual screening enrichments. *J Comput Aided Mol Des* **27**, 221-234

Peptide 1: ARTK(Bio)QTARK(Aoa-RADP)S
Peptide 2: 5Flu-ARTKQTARK(Aoa-RADP)S
Peptide 3: ARTK(Bio)QTARKS
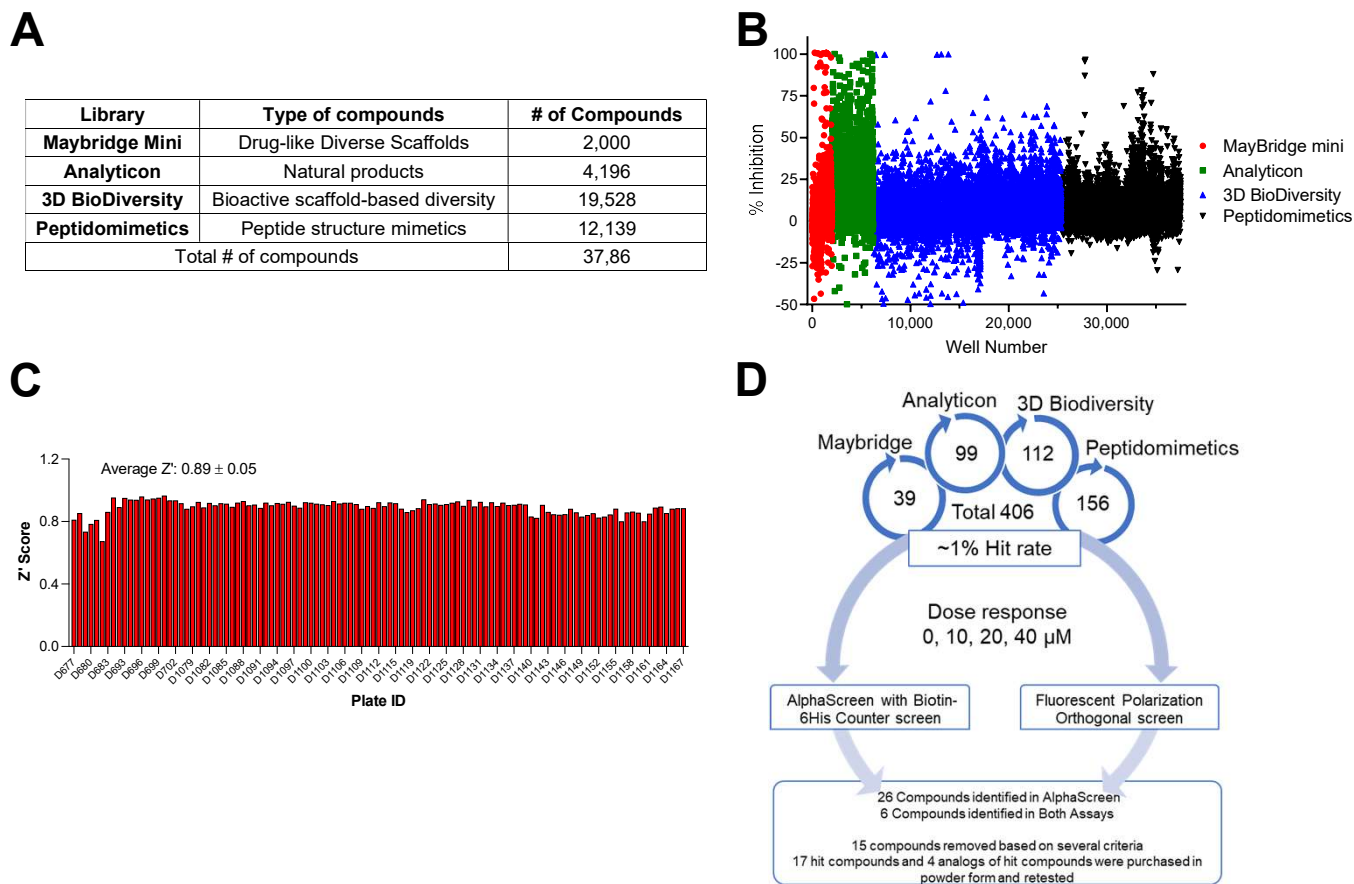Peptide 4: 5Flu-ARTKQTARKS
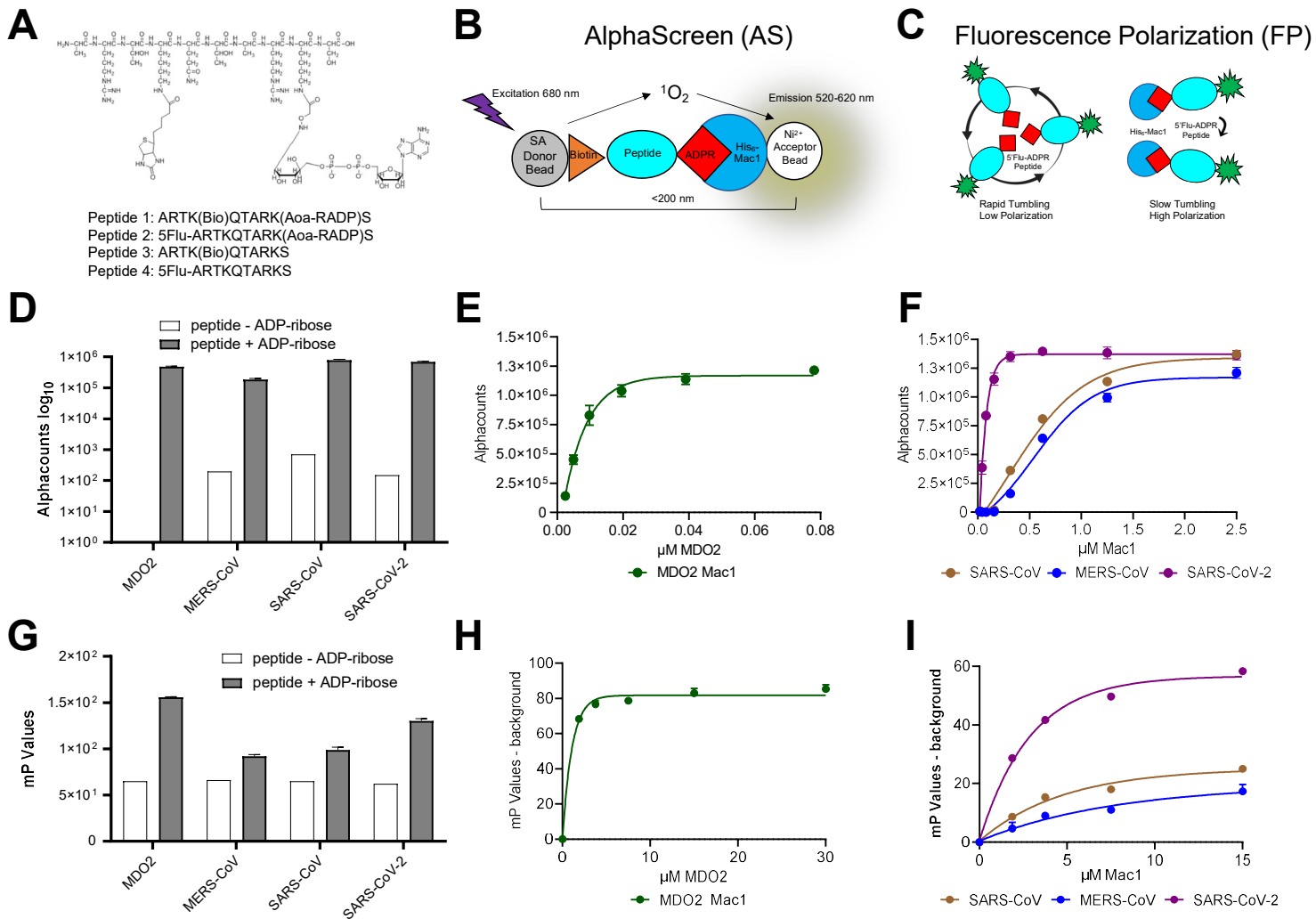
Figure 1. Coronavirus Mac1 binding to ADP-ribosylated peptides. A) Illustration of the amino-oxyacetic acid modified lysine-conjugated ADP-ribosylated peptide with an additional biotin conjugated to a different lysine residue and included are the amino acid sequences and modification sites of peptides used in this study. B-C) Cartoon diagrams depicting a bead-based AS (A) and FP (B) assays for measuring macrodomain interactions with an ADP-ribosylated peptide. D) Macrodomain proteins were incubated with peptide #1 or peptide #3 for 1 hour at RT and Alphacounts were determined as described in Methods. E-F) Peptide #1 was incubated with indicated macrodomains at increasing concentrations and Alphacounts were measured as previously described. G) Mac1 proteins were incubated at indicated concentrations with peptide #2 or peptide #4 and the plate was incubated at 25°C for 1 hr before polarization was determined. H-I) Peptide #2 was incubated with indicated macrodomain proteins at increasing concentrations and polarization was determined as previously described. All data represent the means ± SD of 2 independent experiments for each protein.
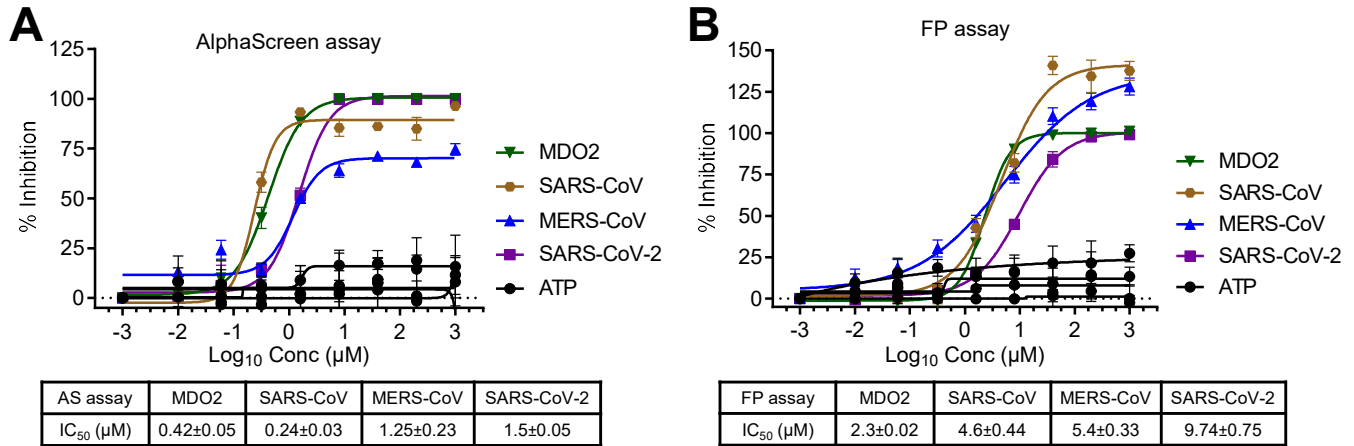
Figure 2. Free ADP-ribose inhibits macrodomain binding to ADP-ribosylated peptides. ADP-ribose competition assays were used to block the interaction between macrodomain proteins and ADP-ribosylation peptides in the AS (A) or FP (B) assays. ATP was used as a negative control. The data represent the means ± SD of 2 independent experiments for each protein.
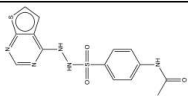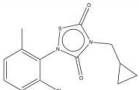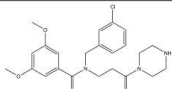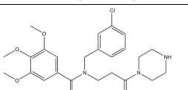
AS assay	MDO2	SARS-CoV	MERS-CoV	SARS-CoV-2
IC_{50} (µM)	0.42±0.05	0.24±0.03	1.25±0.23	1.5±0.05

FP assay	MDO2	SARS-CoV	MERS-CoV	SARS-CoV-2
IC_{50} (µM)	2.3±0.02	4.6±0.44	5.4±0.33	9.74±0.75

A

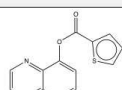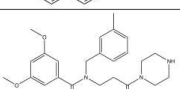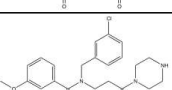| Library	Type of compounds	# of Compounds
Maybridge Mini	Drug-like Diverse Scaffolds	2,000
Analyticon	Natural products	4,196
3D BioDiversity	Bioactive scaffold-based diversity	19,528
Peptidomimetics	Peptide structure mimetics	12,139
Total # of compounds		37,86

B

C

D
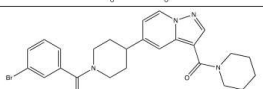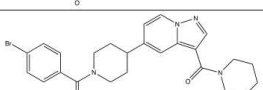
Figure 3. High-throughput screen for SARS-CoV-2 Mac1 inhibitors. A) List of libraries that were screened, the number of compounds from each library, and the type of compounds each library contains. B) Scatterplot showing the % inhibition of each compound in the screen. The cutoff for a hit was the plate median + 3 standard deviations. C) Z' scores were determined for each plate in the screen. The average Z' score was 0.89 ± 0.05. D) Dose response confirmation. From the original screen, we identified 406 potential hits, these hits were retested in a dose-response assay on both the AS and FP assays and were also counterscreened against a biotinylated 6His peptide. After these assays and other exclusion criteria, 17 hit compounds and 4 analogs were repurchased or resynthesized.
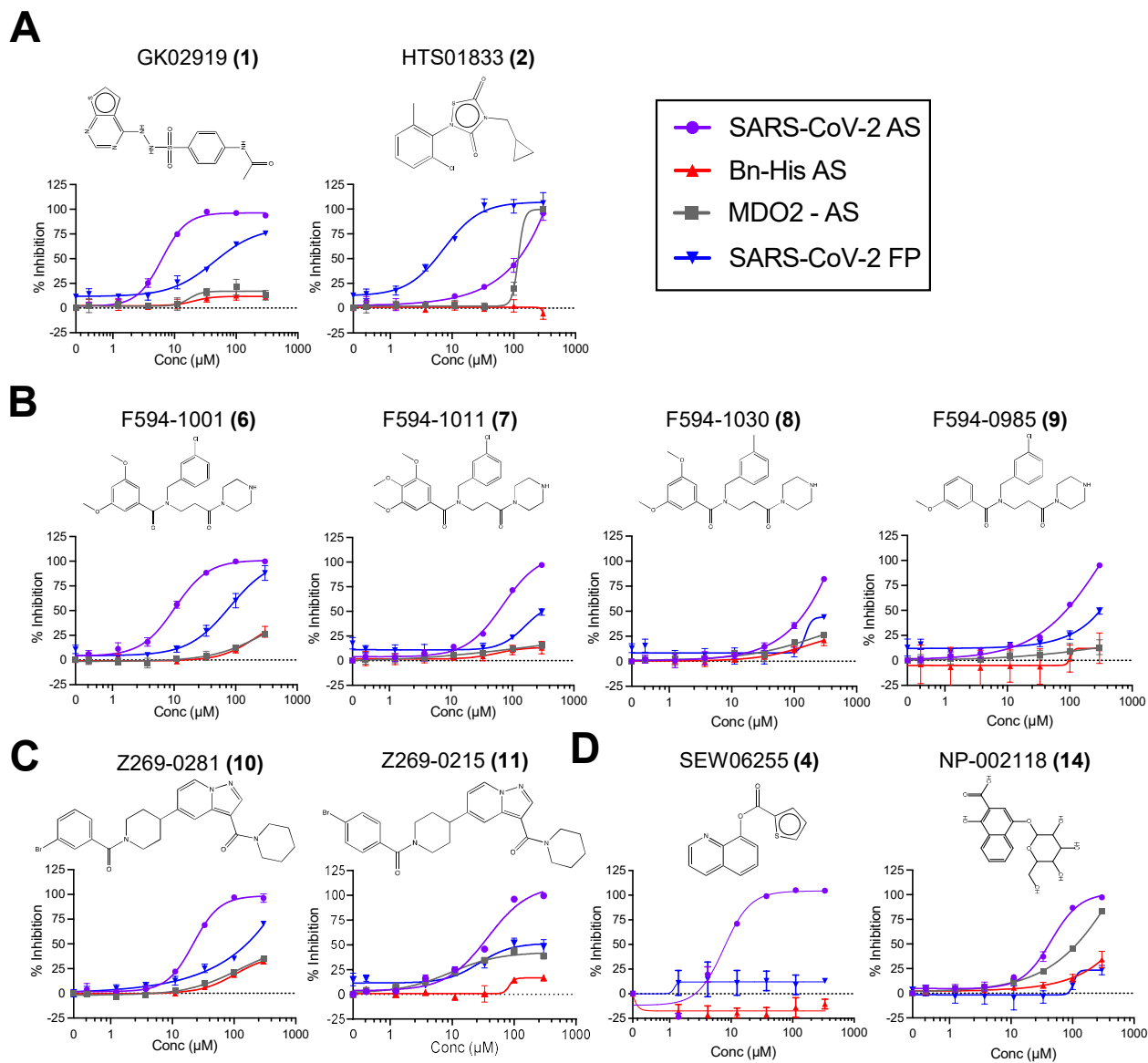
Figure 4. Identification of chemical compounds that inhibit SARS-CoV-2 Mac1 ADP-ribose binding. Dose-response curves representing hit compounds identified in the HTS. A) Maybridge Mini Library compounds **1**, **2**. B) Compound **6** and its analogs, **7**, **8**, **9**. C) Compound **10** and its analog **11**. D) Compounds **4** and **14** which did not inhibit FP assay. Data represent the means ± SD of at least 2 independent experiments for each protein. Structures were created using ChemDraw.

Table 1: IC$_{50}$s of the selected compounds in AlphaScreen and Fluorescence polarization assays

Compound Name	Structure	IC$_{50}$ AS SARS-CoV-2 (µM)	IC$_{50}$ FP SARS-CoV-2 (µM)	IC$_{50}$ AS MDO2 (µM)	IC$_{50}$ AS MERS (µM)
ADP-ribose		1.5 ± 0.05	9.74 ± 0.75	0.42 ±0.05	1.25 ± 0.23
Compounds inhibit both AS and FP					
GK02919 (1)		6.2 ± 0.6	46.88 ± 8.71	NI	39.6 ± 4.2
HTS01833 (2)		104.6 ± 8.4	7.3 ± 1.5	229.6 ± 180.3	>300
F594-1001 (6)		10.3 ± 0.8	81.7 ± 12.3	NI	NI
F594-1011 (7)		70.9 ± 3.5	232.1 ± 118.8	NI	NI
Z269-0281 (10)		26.7 ± 6.5	75.2 ± 10.6	NI	181.3 ± 14.4
Z269-0215 (11)		56.9 ± 33.7	27.6 ± 11.1	NI	181.8 ± 4.7
Compounds inhibit AS only					
SEW06255 (4)		52 ± 3	NI	DND	DND
F594-1030 (8)		368.4 ± 144.7	NI	NI	DND
F594-0985 (9)		78.7 ± 4.3	NI	NI	DND
NP-002118 (14)		45.2 ± 1.9	NI	82.9 ± 4.6	DND

(NI): No Inhibition   (NA): Not Applicable   (DND): Did Not Do
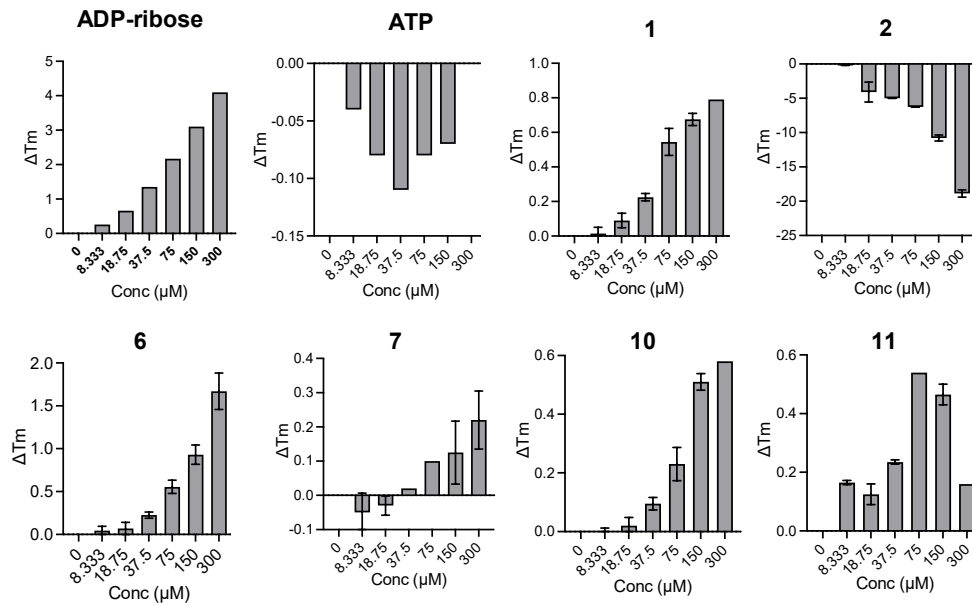
Figure 5. Thermal stability of SARS-CoV-2 Mac1 after incubation with hit compounds. The top 6 hit compounds were tested for their ability to increase the thermal stability of SARS-CoV-2 Mac1 in a differential scanning fluorimetry assay (DSF). The data represent the means ± SD of the ΔT_m from two independent experiments.

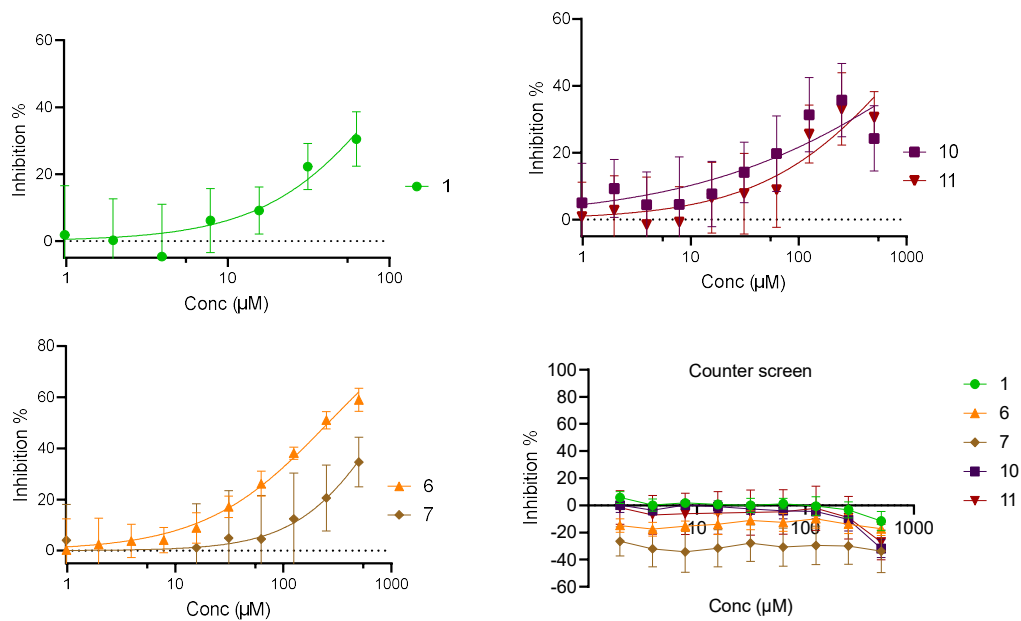Table 2: Peak values of DSF thermal shift temperatures

Compound	Peak ΔTm					
	1	**2**	**6**	**7**	**10**	**11**
Average	0.68	18.88-	1.67	0.22	0.51	0.47
SD	0.04	0.53	0.21	0.08	0.03	0.04
Conc (µM)	150	300	300	300	150	150
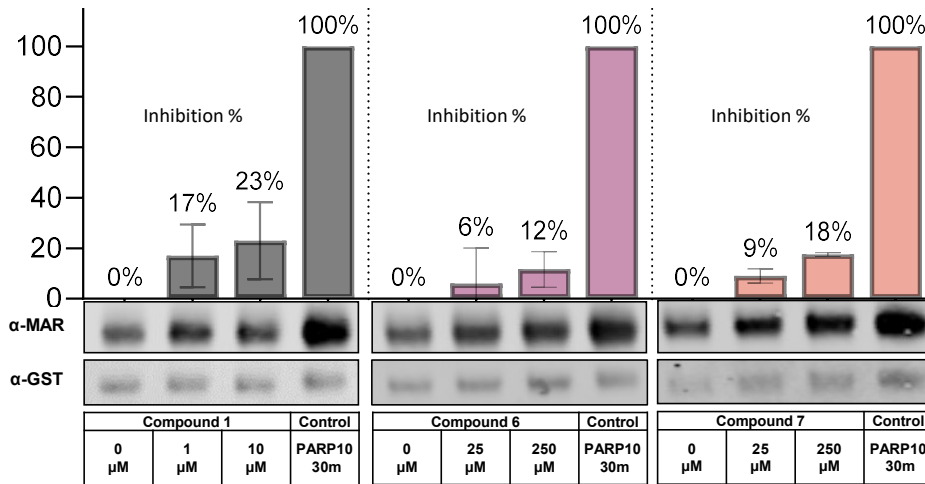
Figure 6. Impact of hit compounds on SARS-CoV-2 ADP-ribosylhydrolase activity. A) Compounds were incubated at indicated concentrations for 30 minutes with the SARS-CoV-2 Mac1 protein prior to adding the PARP10 substrate and then were further incubated for 30 minutes. Proteins were analyzed by Immunoblotting with anti-GST (PARP10) and anti-MAR binding reagent (MABE1076). Gels were quantitated using Image Studio software. The bar graph above each immunoblots represent the mean inhibition ± SD from at least two independent experiments.
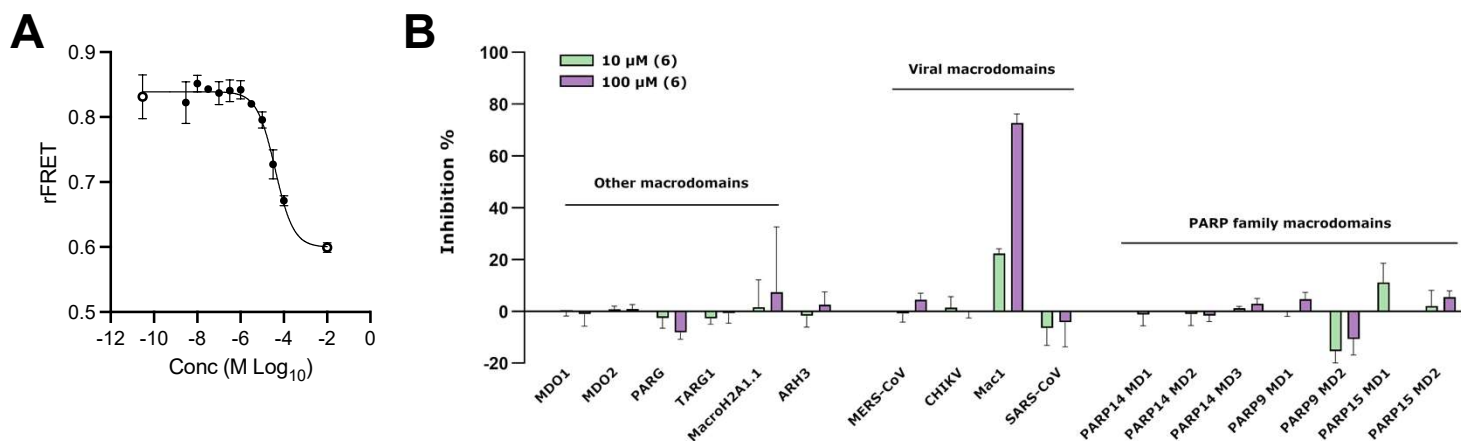
Figure 7. Compound 6 is highly selective for the SARS-CoV-2 Mac1 protein. A-B) Compound **6** was tested in a FRET-based assay for its ability to inhibit SARS-CoV-2 Mac1 protein in a dose-dependent manner (A) and for its ability to inhibit a panel of 17 macrodomain containing proteins (B). The data in means ± SD are shown as a single experiment representative of 3 independent experiments.
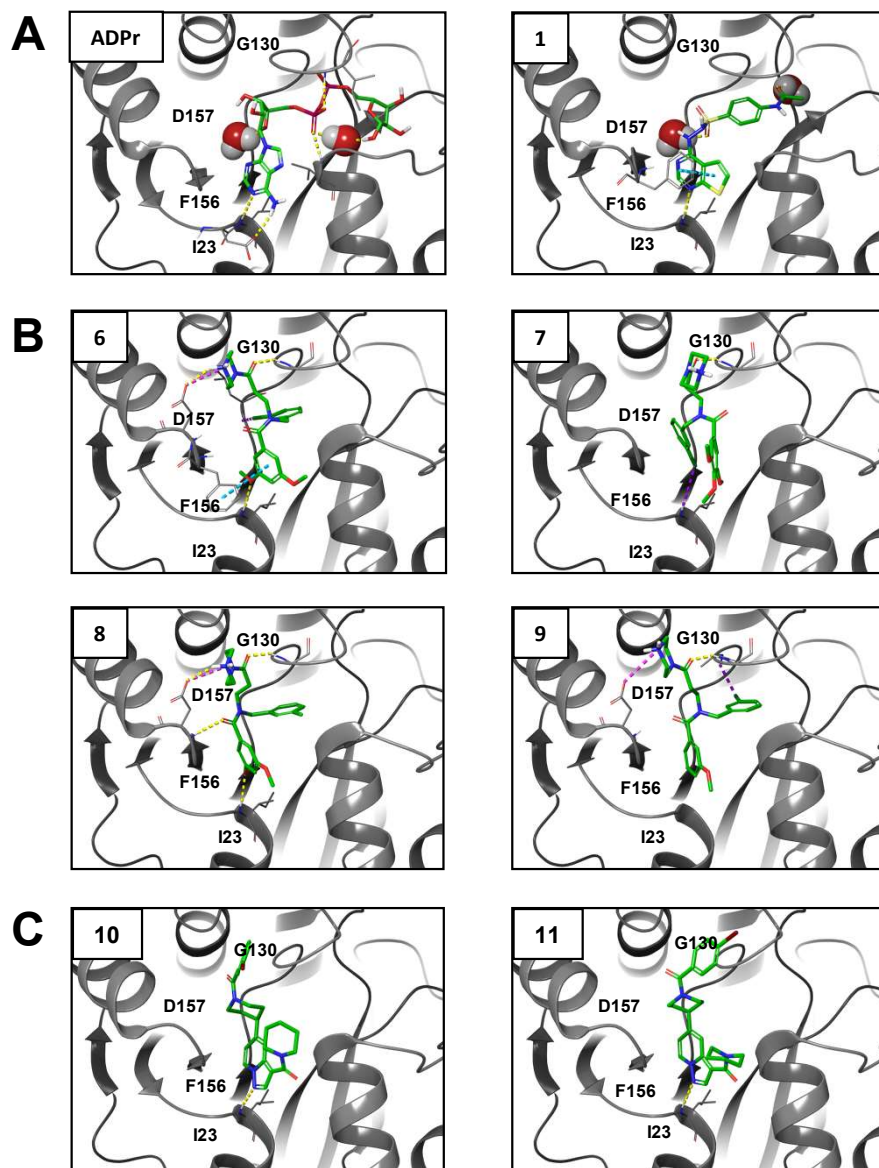
Figure 8. Computational modeling of identified compounds with SARS-CoV-2 Mac1 structures. Indicated compounds were docked and modeled with SARS-CoV-2 Mac1 structures using Maestro Schrödinger software and separated into 3 groups. (A) – Compound 1; (B) Compounds 6, 7, 8, 9; (C) Compounds 10, 11. Yellow lines - hydrogen bonds; Cyan lines - pi-pi interactions; magenta lines – weak hydrogen bonds; and purple lines – halogen bond.

Table S1: Compound docking scores

Compound #	docking score	glide emodel	Mac1 Structure
1	-7.857	-81.695	6WOJ
6	-4.563	-50.414	7RK0
7	-3.338	-34.249	7RK0
8	-4.064	-57.015	7RK0
9	-4.287	-61.816	7RK0
10	-4.806	-59.941	6WEY
11	-5.306	-58.757	6WEY
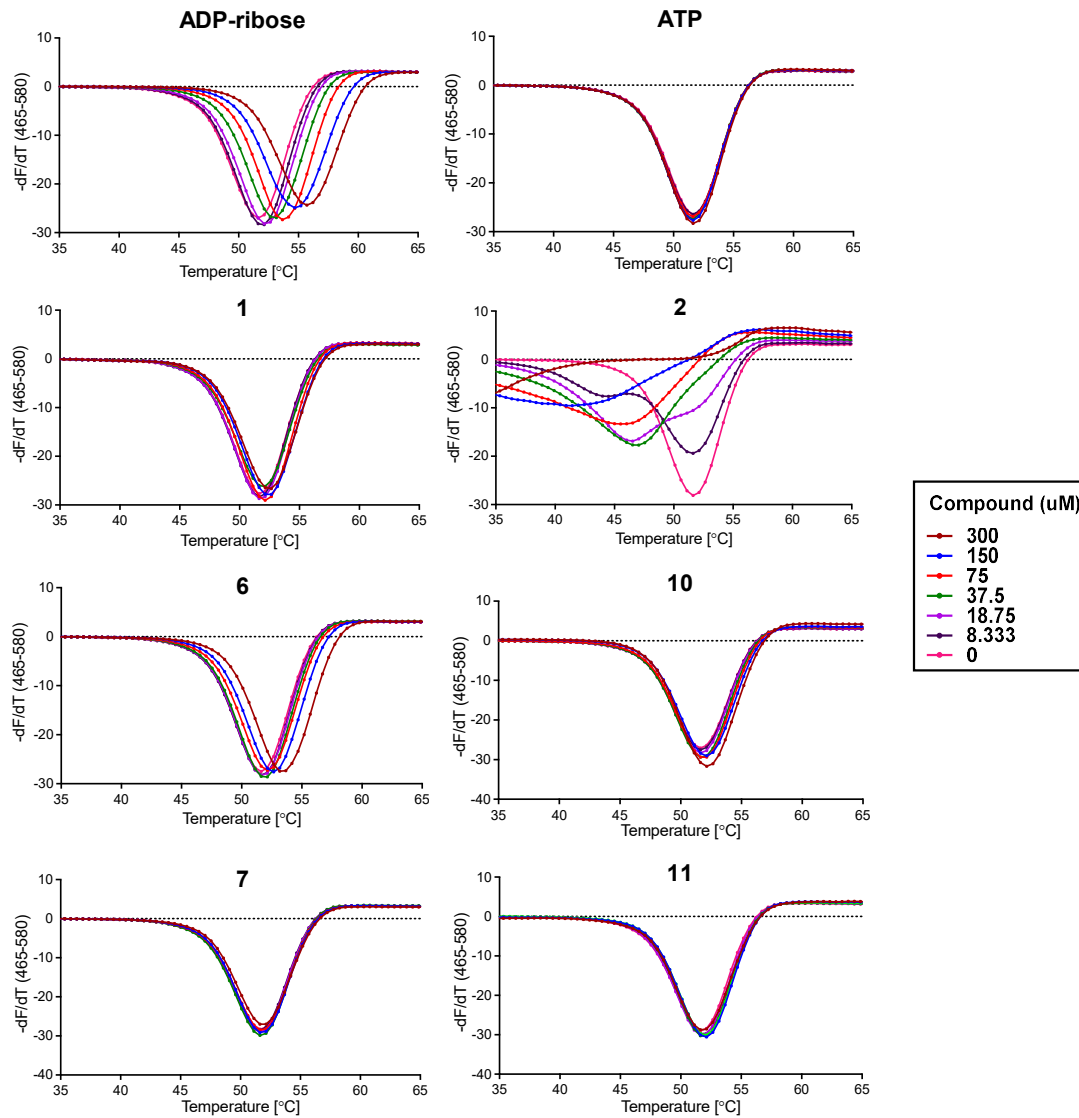
Figure S1. Thermal stability of SARS-CoV-2 Mac1 after incubation with hit compounds. The top 4 hit compounds were tested for their ability to increase the thermal stability of SARS-CoV-2 Mac1 in a differential scanning fluorimetry assay (DSF). Thermal profiles are shown for each compound at different concentrations. \
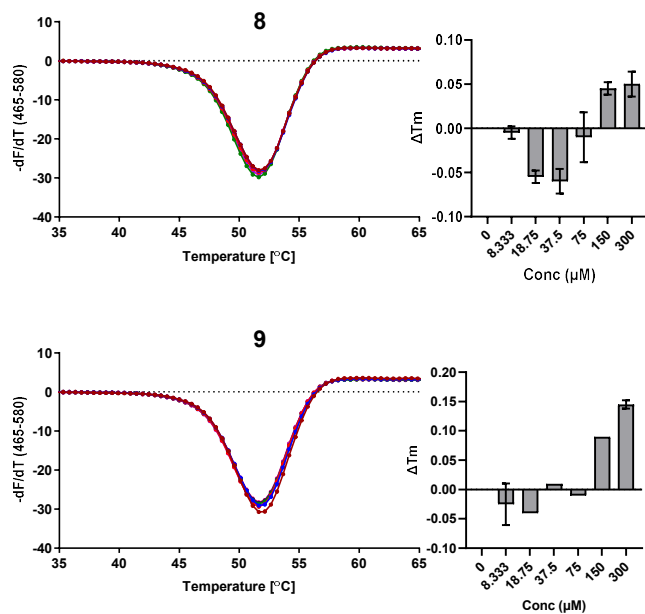
Figure S2. Thermal stability of SARS-CoV-2 Mac1 after incubation with analog compounds. Two analogs of FS2MD-006 are shown here for their ability to increase the thermal stability of SARS-CoV-2 Mac1 in a differential scanning fluorimetry assay (DSF). Thermal profiles and change in T_m are plotted for each compound at different concentrations.